Faraday Discussions

Cite this: *Faraday Discuss.*, 2025, **261**, 359

PAPER

Silica biomineralization in plants alters the structure of lignin†

Srinath Palakurthy, [a] Michael Elbaum [b] and Rivka Elbaum *[a]

Received 19th January 2025, Accepted 13th February 2025
DOI: 10.1039/d5fd00011d

Biomineralization of silica is a major process in plants, which may contribute 3–10% of tissue dry weight. For reasons that remain unclear, plants containing silica are less sensitive to abiotic and biotic stress. In particular, the mechanisms of silica deposition and stress amelioration are still not fully understood. Silica resides mostly in the extracellular volume (the apoplast) which is made of the lignocellulosic cell wall. In a previous work we showed that synthetic lignin catalyses the formation of silica nanoparticles at RC-OSi(OH)$_3$ positions. Since the phenolic O-4 position is the most reactive during lignin polymerization, the binding sites form at the expense of β-O-4 lignin backbone bonds. Therefore, synthetic lignin becomes more branched when polymerized in the presence of silicic acid, as compared to lignin polymerized without silicic acid. To study lignin–silica relationships in the plant, we extracted lignin from stems of wild type sorghum and compared it to lignin extracted from mutants exhibiting high and low silica contents. The thermal stability of both non-extracted biomass and extracted lignin was measured using thermogravimetric analysis (TGA). High-silica biomass was thermally less stable than low-silica biomass, suggesting lower content of ether (β-O-4) linkages. This interpretation was supported by gas chromatography-mass spectroscopy (GC-MS). Fourier transform infrared (FTIR) and X-ray photoelectron spectra (XPS) indicated lignin with C–O–Si modifications in all genotypes and further showed silicic acid binding to lignin phenolics and carbonyl moieties. Our results show that lignin extracted from genotypes with native-silicon levels have higher affinity to silicic acid, catalysing silica deposition through Si–O-4 (Si–

[a]*The Robert H. Smith Institute of Plant Sciences and Genetics in Agriculture, The Hebrew University of Jerusalem, 7610001 Rehovot, Israel. E-mail: rivka.elbaum@mail.huji.ac.il*

[b]*Weizmann Institute of Science, 7610001 Rehovot, Israel*

† Electronic supplementary information (ESI) available: Production and isolation of a sorghum line carrying both *bmr6* and *lsi1* mutations (SI1), lignin extracted using alkali pretreatment process (SI2), a representative GC-MS chromatogram of trimethyl-silyl (TMS) derivatives of sorghum genotype thioacidolysis products (Fig. S1), high resolution XPS Si 2p spectra of lignin+Si from WT, *lsi1*, *bmr6* and *bmr6*×*lsi1* sorghum genotype at silicic acid concentration of 2.5 mM (Fig. S2), thermal decomposition behaviour of lignins reacted with different concentrations of silicic acid in phosphate buffer solution (Fig. S3), FTIR transmission spectra of lignin extracted using alkali pretreatment process (Fig. S4), tomographic sections of the high silicon specimen (*bmr6* + 2.5 mM Si), scale 1.5 nm per pixel (Movie 1), tomographic sections of the low silicon specimen (*bmr6*×*lsi1* + 2.5 mM Si), scale 1.5 nm per pixel (Movie 2). See DOI: **https://doi.org/10.1039/d5fd00011d**

phenoxyl) bonds, and suggest that the presence of silicic acid during *in vivo* lignin polymerization reduces β-O-4 ether linkages.

1. Introduction

Biomineralization, the process by which organisms produce minerals, is indeed found in a wide variety of organisms, including plants, fungi, bacteria, and animals. The self-amplifying nature of biomineralization is particularly fascinating, as it involves a feedback loop in which small initial mineral particles or structures gradually grow into larger and more complex structural supports (*e.g.*, shells, skeletons, bone and teeth). This synergistic response helps organisms to maximize their survival, contributing to both growth and survival in a dynamic and changing environment. Mineral formation by organisms is usually carried out in an aqueous environment at atmospheric pressure and temperature, and involves organic biomacromolecules that self-organize into highly ordered structures under regulation of the organisms. These macromolecules act as templates that control the morphology and molecular/atomic structure of mineralised phases. These hybrid structures of organic and inorganic materials have unique functions not seen in single-component materials. Therefore, understanding the biomineralization process can promote novel methods for the production of green functional materials to meet the needs of modern society.[1–3]

Plants growing in silica-rich soil take-up soluble silicic acid from the soil solution and transform it into solid amorphous silica. Silicic acid moves with water in the extracellular space, called the apoplast, which is made of

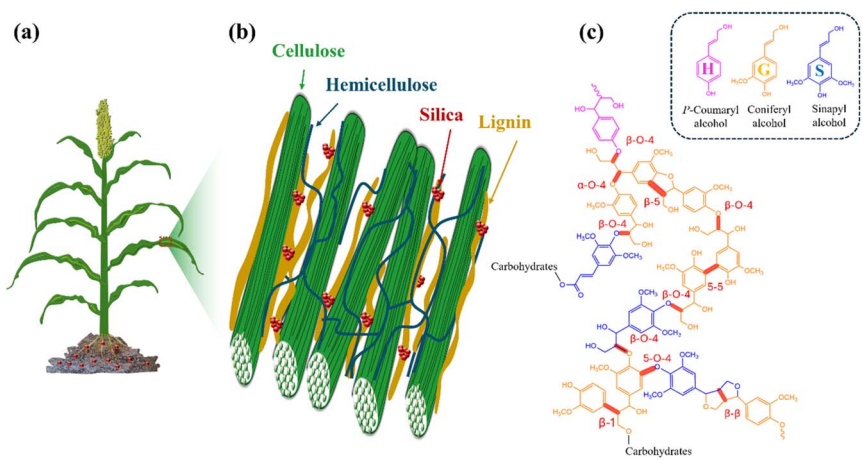

Fig. 1 Cell wall model, demonstrating silica deposited into the cell wall matrix. (a) Sorghum plant planted in silicate (red) soil which contains silicic acid available for root intake. The bulk of silicic acid resides in the apoplast, *i.e.* the extracellular space, and moves with the water transpiration stream to the shoot. (b) Silica deposits (red) in the cell wall, onto a lignin (orange)–hemicellulose (blue) matrix that binds cellulose microfibrils (green). (c) Lignin model structure, made of three canonical monomer units, H, G, and S, bound *via* β-O-4 backbone connection and other phenylpropanoids *via* a random radical-driven dehydrogenation. β-O-4 are the most abundant linkages in natural lignins.[5]

lignocellulosic cell walls and voids. With the help of the transpiration stream and dedicated protein transporters,[4] silicic acid is distributed in the plant body and gets deposited mostly at the epidermis of leaves and stems (Fig. 1).[6] The organic environment of cell walls, including abundant proteins, polysaccharides (cellulose and hemicellulose), and phenolic (lignin) compounds, is likely to play an ultimate role in the formation of silica.[7] A few reports suggest that silicon (Si, as silicic acid or silica) affects the composition of plant cell walls *in vivo*[8–10] and *in vitro*, by binding to phenolic components in polymerization reactions.[11] Reciprocally, silica formation was linked with lignin formation *in vitro*[12–14] and *in vivo*.[15,16] However, the molecular details explaining lignin-assisted biosilicification in plants are incomplete.

The simplified *in vitro* system of peroxidase-catalyzed polymerization of lignin model compounds shows that silica is precipitated by polymerizing lignin, but not by lignin monomers, and that silica prevents the formation of large lignin fragments.[11,12] We have shown that silicic acid binding at the phenoxyl radical/quinone methide moieties of lignin reduces alkyl-aryl ether (β-O-4) backbone linkages in the final lignin. Synthetic lignin catalyses silica deposition through covalent Si–O–C bonding, which leads to the growth of 2–5 nm silica particles.[17]

In plants, lignin is secreted into a cellulose–hemicellulose structure in secondary cell walls. Pure lignin typically accounts for 15–30% of lignocellulosic biomass. It is covalently linked to hemicellulose, usually by ester bonding, and thereby crosslinks polysaccharides, providing mechanical strength and rigidity to the cell wall (Fig. 1).[18–20] Delignification, the process of extracting lignin during pulping pretreatment procedures, disrupts the glycosidic bonds in polysaccharides. As a result, hydrolysable linkages in lignin may break as well.[21] Lignocellulosic biorefinery technologies have developed a process using acetic and formic acid-based organosolv fractionation of lignin from biomass without degradation or extensive modification.[22,23] This method adds carboxylic acid groups to extracted lignin molecules through esterification (acetate and formate) that are cleavable upon hydrolysis.[24,25]

Sorghum is a highly productive grain staple crop, tolerant to drought and salinity.[26] Sorghum biomass is also a research target for developing second-generation biofuels that do not compete with food production.[27] The high silicon accumulation in sorghum may interfere with its dual role as food and fodder/biofuel source.[28] Further, sorghum is a model plant for studying silica deposition.[29] As such, a sorghum mutant carrying a defective gene for silicon root transporter – *Sblsi1*, was isolated, which absorbs about 200 times less silica as compared to the wild type (WT) plant.[30]

In the present work, the *in planta* lignin–silica relationship was studied by analysing the lignin of native- and low-silicon (*Sblsi1*) sorghum genotypes. We compare the effects of Si uptake in the background of both wild type (WT) and a lignin mutant presenting extra aldehyde at the expense of hydroxyl lignin groups (brown mid-rib 6, *bmr6*[31]). The pyrolysis behaviour of unextracted biomass and of acid-based organosolv isolated lignin, indicated a higher content of native aryl-alkyl ether (β-O-4) linkages in low-silicon genotypes. Lignin extracted from high silicon genotypes had higher catalytic activity in silicic acid polymerization, as compared to lignin extracted from low-silicon genotypes. We identified Si–O–C bonds that formed during lignin synthesis *in planta* and suggest that these positions catalyse formation of SiO_2 nanoparticles.

2. Materials and methods

2.1 Materials and reagents

Formic acid (FA, reagent grade, ≥95%, Sigma-Aldrich) and glacial acetic acid (AA, Reagent Plus, ≥99%, Sigma-Aldrich) were used in lignin extractions. Dipotassium hydrogen orthophosphate (K_2HPO_4) and potassium dihydrogen phosphate (KH_2PO_4) were used to prepare 0.1 M potassium phosphate buffer solution at pH 7.4. 1 M. Silicic acid was produced by adding 150 μL tetramethyl orthosilicate (TMOS, Sigma-Aldrich) to 850 μL 1 mM hydrochloric acid (HCl, ACS reagent, 37%, Sigma-Aldrich), and mixing for 30 min. Boron trifluoride diethyl etherate (>46.5% BF_3, Sigma-Aldrich), ethanethiol (99+%, Thermo Scientific), 1,4-dioxane (99.8%, Sigma-Aldrich), bisphenol-A (≥99%, Sigma-Aldrich), sodium bicarbonate ($NaHCO_3$, 99.5%, Merck), and ethyl acetate (99.9%, Sigma-Aldrich) were used in thioacidolysis.

2.2 Plant materials

Sorghum bicolor (L.) Moench, line BTx623 (wild type, WT), low-silicon mutant (*Sblsi1*), with about 1 : 200 silica content in relation to WT plants,[30] and brown midrib (*bmr6*) containing altered lignin composition,[31] were grown in a green house. In addition, we produced a cross between *bmr6* and *Sblsil* (*bmr6*×*lsi1*), F1 hybrid, and propagated it *via* self-fertilization to F2 inbred lines. Selection of the F2 line carrying both *bmr6* and *Sblsi1* mutations was done based on PCR amplification of the mutated genes (ESI SI1†). Plants mutated at both *Sblsi1* and *bmr6* were grown in parallel to the other genotypes. No visual variation in growing parameters was detected between the four genotypes. Stems of approximately 3 month-old plants were collected, cut into less than half-centimetre pieces, and thoroughly washed under running tap water and then distilled water. The washed pulp was dried in an oven at 70 °C for 3 days. The final dried samples were stored for later use.

2.3 Determination of silica content in biomass

Approximately 2 grams of chopped and dried sorghum stems were placed in a muffle furnace using porcelain crucibles and heated at 600 °C for 12 h. The ash was collected and treated with 1 M HCl and washed once with distilled water. The final acid insoluble ash (AIA) was weighed, AIA was considered to be mainly silica, and its percent per dry weight biomass was calculated.[32]

2.4 Isolation of lignin

The lignin fraction was extracted by mixing 1 g (dry matter) of chopped sorghum stems in a volume of 10 mL acetic acid/formic acid/water medium (AA/FA/H_2O: 55/30/15 volume ratio).[23] It was pre-soaked for 30 min at 50 °C on a heating plate. After soaking, the mixture was kept at 100 °C for 2.5 h with continuous stirring. The mixture was allowed to cool down to room temperature and then filtered with a vacuum filter funnel assembled with a filter disk (11 μm pore size; Whatman filter paper). Acids were evaporated from the filtrate fraction containing the extract liquor until they reached around 60% volume by vacuum evaporation (320 mbar). Distilled water was added to the concentrated extract liquors while

stirring, to increase the solution pH from a baseline value below 1 to precipitate the lignin at around pH 2. We noted that the water/concentrated liquor ratio to achieve optimal lignin precipitation was 2/1 for WT and *bmr6* and 4/1 for *lsi1* and *bmr6*×*lsi1*. The precipitates were recovered by centrifugation and washed once with phosphate buffer (pH 7.4) and two times with distilled water.

2.5 Lignin–silicic acid precipitation process

Isolated never-dried lignin particles (approximately equal to the dried weight of 3 mg) were dispersed in 3.8 mL of 0.1 M phosphate buffer solution at pH 7.4. Silicic acid at final concentrations of 2.5 and 5 mM was added to the solution and agitated at 200 rpm for 3 days in the dark. Samples were centrifuged at 9000 rpm and the precipitate was washed 3 times with double distilled water, and dried under vacuum at room temperature.

2.6 Characterization

2.6.1 Thermogravimetric analysis (TGA). About 10 mg of sample (dried biomass or isolated lignin samples that were dried under vacuum in a desiccator) was placed in platinum crucibles and linearly heated from ambient room temperature to 900 °C at a rate of 10 °C min^{-1} in a thermogravimetric analyser (TGA-Q500 series, TA instruments). Nitrogen gas at a flow rate of 90 mL min^{-1} was used to purge the system and also provided an inert atmosphere for the experiments.

2.6.2 Gas chromatography-mass spectrometry (GC-MS). Thioacidolysis reactions were performed according to a previously published procedure.[33] The plant materials were ground into powder in liquid nitrogen and then vacuum dried overnight. 2 mg of dry ground biomass were accurately weighed into a 2 mL Teflon-lined screw-cap micro-reaction vessel. Thioacidolysis reagent was prepared by mixing 2.5% boron trifluoride diethyl etherate, 10% ethanethiol and 87.5% dioxane by volume. Bisphenol-A was added as an internal standard at a concentration of 0.05 mg mL^{-1}. One mL of thioacidolysis reagent was added to each vial containing the biomass and the vials were tightly capped. The reaction was run at 100 °C for 4 h, quenched by cooling on ice for 5 min, and vortexed. The insoluble residue was allowed to settle, and 400 μL of the supernatant was transferred into 4 mL glass vials. 250 μL of 1 M aqueous sodium bicarbonate solution, 125 μL of 2 N HCl, 1000 μL double distilled water, and 500 μL ethyl acetate were added sequentially and the samples were vortexed to ensure mixing. The oily organic layer obtained was subjected to GC-MS analysis (GCMS-350). The trimethylsilyl derivatives of lignin monomers were identified and quantified relative to the internal standard.

2.6.3 Fourier transform infrared (FTIR) spectroscopy. Isolated lignin and lignin–silicic acid samples were dried under vacuum in a desiccator. Pellets for analysis were prepared by mixing ~1 mg of dry powdered samples with ~99 mg of KBr. Fourier transform infrared (FTIR) spectra were obtained in transmittance mode using a Nicolet 6700 FTIR spectrometer (Thermo Fisher Scientific, Inc), with 20 spectral scans in the range 400 to 4000 cm^{-1} with a resolution of 4 cm^{-1}. Peak fitting analysis was performed on the FTIR absorption spectra using Lorentz peak fitting, with absorbance calculated as a logarithmic function of transmittance (absorbance $= 2 - \log 10\ (\%T)$). The relative change in the integrated absorption

area of the deconvoluted absorption bands was calculated as the difference between the normalized (peak area/total area of fitted range) peak area.

2.6.4 X-ray photoelectron spectroscopy (XPS). X-ray photoelectron spectroscopy (XPS) measurements were performed on a K-alpha XPS system (Kratos, Kratos Analytical Ltd) using high-resolution monochromatic Al Kα X-ray as the excitation source. Isolated lignin and lignin–silicic acid samples were dried under vacuum in a desiccator. Dry samples were excited by Al Kα X-rays ($h\nu = 1486.7$ eV) with a working voltage of 15 kV and an emission current of 40 mA. Multiplex (narrow) high-resolution spectra of the C 1s, O 1s and Si 2p regions were collected. The spectra were analysed using built-in Kratos software.

2.6.5 Scanning electron microscopy-energy-dispersive X-ray spectroscopy (SEM-EDS). The structural morphology and elemental composition were studied using a high-resolution scanning electron microscope (HR-SEM, JSM-7800f) jointly equipped with energy-dispersive X-ray spectroscopy (EDS). A drop of ~5 μL of isolated lignin and lignin–silicic acid precipitates were drawn, deposited onto carbon tape mounted on an aluminium stub, and then dried at room temperature. Images of dry samples were collected using a secondary electron detector on AuPd sputter-coated samples with 2.00 kV beam energy and 4.00 mm working distance.

2.6.6 Scanning transmission electron tomography and EDS. Specimens were prepared on 200 mesh Cu C-flat grids (Protochips, USA) by drop-casting 5 μL of the material suspended in deionized water, followed by gentle air-drying. The electron microscope, a Tecnai T20-F (FEI Inc, USA), was operated at 200 kV acceleration in the STEM microprobe mode with a 30 micron C2 aperture (for 0.8 mrad semi-convergence angle). The detector was an ARINA (DECTRIS SA, Switzerland) hybrid pixel camera, operated in parallel with the standard high angle annular dark field detector, both controlled by a custom scan generator.[34] Camera length was 100 mm and pixel size was 1.54 nm. Probe current was 10 μA and 6.5 μA for the *bmr6* and *bmr6*×*lsi1* samples, respectively. While samples were prepared and dried at room temperature, tomography was performed under cryogenic conditions in order to suppress carbon contamination in the microscope vacuum. Low-dose protocols were followed in order to avoid warping and distortion of the lignin assemblies. Tomographic series were recorded in a dose-symmetric mode covering the range −60 to 60° in 3° steps and aligned by patch tracking in IMOD.[35] A signal representing the integration of the central disk projected to the camera, *i.e.*, the incoherent bright field image, was reconstructed by SIRT with 100 cycles using Tomo3D.[35] Contrast was inverted in preparation of Fig. 10, with mapping of dark values to partial transparency so as to reveal the strongly scattering nanoparticles embedded within the lignin matrix.

Energy-dispersive X-ray spectroscopy measurements were acquired in a Talos 200-X microscope (Thermo-Fisher Scientific) equipped with a QUANTAX Flat-QUAD spectrometer (Bruker). As above, the measurements were performed under cryogenic conditions. Data were analysed using the embedded Velox software.

3. Results and discussion

3.1 Variations in biomass composition of four sorghum genotypes

To understand the effect of silicic acid and silica on lignin structures, we grew sorghum wild type (WT) plants, mutants in lignin biosynthesis (*brown midrib 6*,

Table 1 Fractionation of sorghum stems into silica and organic phases. Percentage silica per biomass dry weight was measured by weighing the acid insoluble ash (AIA). Percent weight per biomass or per isolated lignin dry weight are calculated based on thermal gravimetric analysis (TGA) (Fig. 2). Stage (i): residual water loss, stage (ii): polysaccharides decomposition and lignin interunit linkages and side chain breaking, stage (iii) (biomass) or residue (lignin): carbonization

		Thermal gravimetric analysis (TGA)									
		Biomass						Lignin			
		Stage (i) (40–170 °C)		Stage (ii) (170–480 °C)		Stage (iii) (480–900 °C)		Stage (ii) (170–480 °C)			
Sorghum genotype	Silica (% weight per biomass dry weight)	Weight loss (%)	Peak (°C)	Weight loss (%)	Peak (°C)	Weight loss (%)	Peak (°C)	Weight loss (%)	Peak 1 (°C)	Peak 2 (°C)	Residue (%)
WT	2.0 ± 0.2	3.4	154	56.7	316	21.1	~600	55.2	256	353	23.3
lsi1	0.04 ± 0.02	5.8	160	59.9	343	10.7	~600	57.5	269	363	28.1
bmr6	2.3 ± 0.2	5.6	154	55.7	320	11.8	~600	57.2	254	338	23.3
bmr6×lsi1	0.3 ± 0.1	8.7	154	53.2	331	8.5	~600	59.2	263	342	25.8

bmr6 [31]), and mutants in silicic acid intake (low silicon 1, *lsi1* [30]). We also produced double mutant plants by crossing a mutant in *bmr6* with a mutant in *lsi1* (*bmr6*×*lsi1*, see SI1† for details). Silica content was measured in the stems (Table 1). As expected, a much lower percentage of silica was observed in the biomass of both low-silicon genotypes (*lsi1* and *bmr6*×*lsi1*, herein BM-LowSi) as compared to the genotype with native-silicon intake (WT and *bmr6*, herein BM-HighSi). Furthermore, a slightly higher percentage of silica was observed in both lignin mutants (*bmr6* and *bmr6*×*lsi1*) as compared respectively to plants with native lignin (WT and *lsi1*), in accordance with published results.[16]

The thermal gravimetric analysis (TGA) of stems from flowering plants presented a three-stage decomposition process, with distinct weight loss rates, as seen by differential thermal gravimetry (DTG) (Fig. 2a, b and Table 1): (i) moisture loss (40–170 °C); (ii) lignin rapid devolatilization (170–480 °C) and polysaccharide decomposition (220–480 °C) including hemicellulose (220–310 °C) and cellulose (300–480 °C); and (iii) char formation (>480 °C), where the carbonaceous lignin reduced to graphite.[36] A shift of the polysaccharide decomposition (stage (ii)) to higher temperatures was detected in the BM-LowSi as compared to BM-HighSi (Table 1). This could indicate increased crosslinking in the low-silicon cell walls, pointing to changes in lignin structure (see Fig. 1).[37] Furthermore, the mass which was lost during char formation (stage (iii), >480 °C) was lower in BM-LowSi as compared to BM-HighSi (Table 1). This could result from the possible role of silica in facilitating reduction and evaporation of lignin radicals.[17]

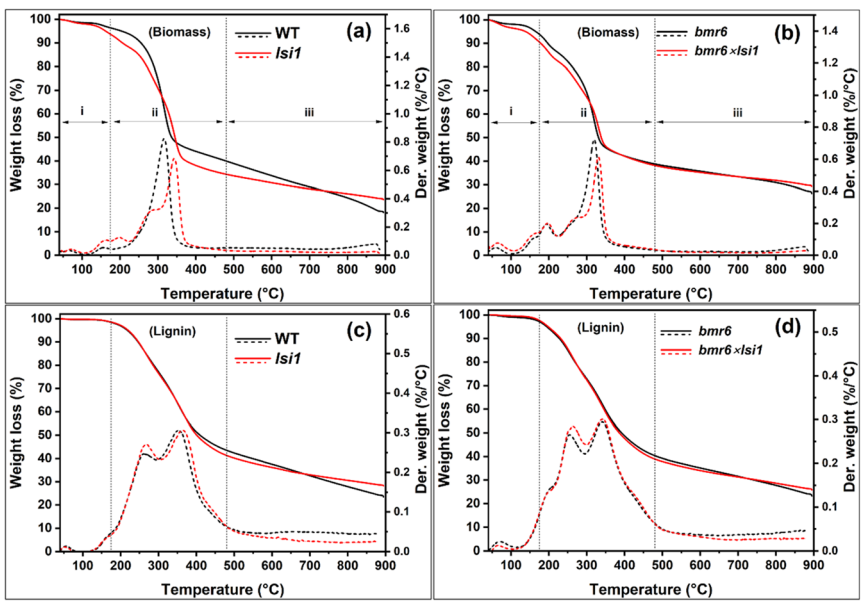

Fig. 2 Thermal decomposition of biomass (a and b) and isolated lignin (c and d) from stems of four sorghum genotypes. Biomass thermal degradation (continuous lines) and degradation rates (dotted lines) of (a) WT (black) compared to low silicon *lsi1* (red), and (b) lignin mutant *bmr6* (black) compared to low silicon lignin mutant *bmr6*×*lsi1* (red). Thermal degradation and degradation rates of lignin extracted from stems of (c) WT (black) and *lsi1* (red), and (d) *bmr6* (black) and *bmr6*×*lsi1* (red). Degradation was divided into stages (i)–(iii), and % weight of each stage was calculated (Table 1).

To further confirm the increase in crosslinking and other possible changes in lignin structure in BM-LowSi (herein Lig-LowSi) in comparison to lignin in BM-HighSi (herein Lig-HighSi), lignin monomers were isolated *via* thioacidolysis of the biomass, and β-O-4 cleavage derived monomers were quantified by GC/MS (Fig. S1†). Thioacidolysis relies on the selective cleavage of β-O-4 ether linkages to produce thioethylated H, G and S monomers (see inset of Fig. 3).[38,39] G and S-derived monomers were the major products in all genotypes, while H-derived monomers were detected at trace levels. The yield of monomers and S/G ratio derived from lignin mutants *bmr6* and *bmr6×lsi1* were lower compared to WT and *lsi1* genotypes (Fig. 3), in agreement with published analyses of lignin composition in the *bmr6* sorghum genotype.[31] All three monomer yields obtained from BM-LowSi were higher than those obtained from BM-HighSi, similar to published data.[10] This could be interpreted as an increase in the lignin fraction in the BM-LowSi relative to BM-HighSi. However, our TGA results do not show such trends (Fig. 2a, b and Table 1). Therefore, we relate this variation simply to increased β-O-4 linkages in the BM-LowSi as compared to BM-HighSi, similar to synthetic lignin produced *in vitro*.[17]

3.2 Variation in structure of extracted lignin

To highlight the effects of silicic acid or silica on lignin structure, lignin was isolated from the stem's biomass by acid based organosolv extraction. Scanning electron micrographs (SEM) of isolated lignins showed spherical lignin particles of 10 to 50 nm in diameter that aggregated into a porous mesh (Fig. 4). Lignin extracted from *bmr6* mutants (*bmr6* and *bmr6×lsi1*) aggregated into a finer mesh,

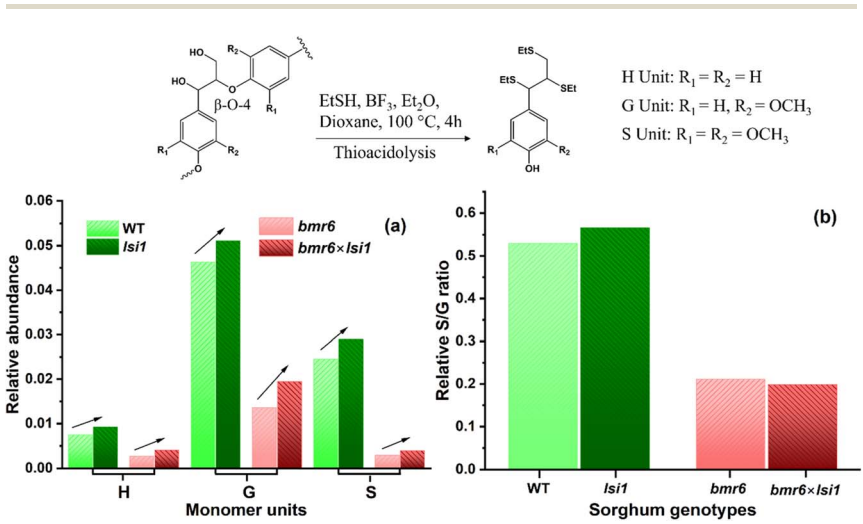

Fig. 3 Distribution of major lignin units in stems of sorghum genotypes quantified by GC-MS following thioacidolysis. (a) Abundance of monomer units calculated by measuring peak area of ions relative to an internal standard. Arrows demonstrate a trend of increased monomer release in BM-LowSi (dark shadow) as compared to BM-HighSi (light shadow) in native (green) and mutated (red) lignin genotypes. (b) Calculated monomer S/G ratio. Color-codes are similar to panel (a). Inset: representative chemical reaction of the formation of thioethylated H, G and S monomers by the cleavage of β-O-4 ethers in lignin.

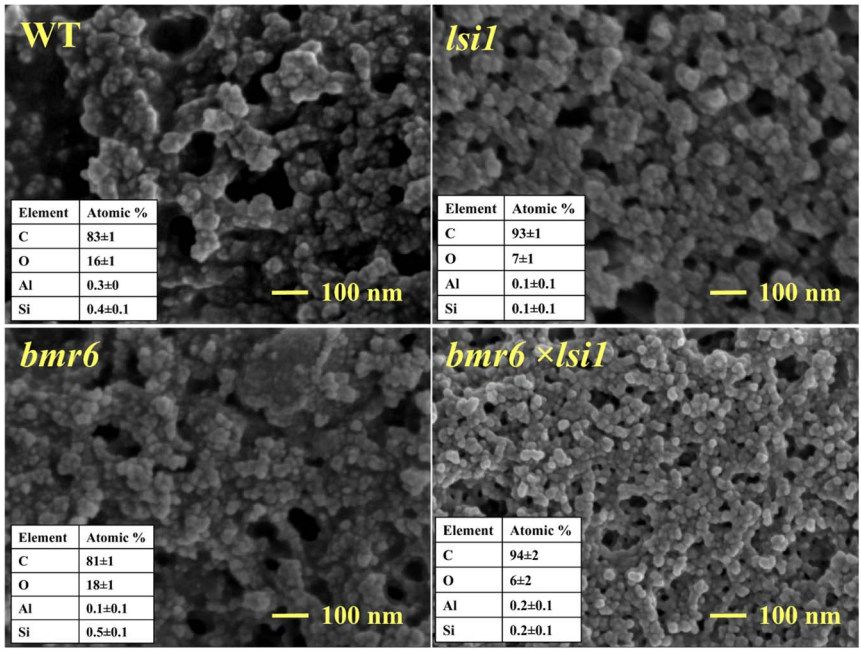

Fig. 4 Scanning electron micrographs of lignin extracted from the four sorghum genotypes, as marked on the images. Insets: tabulated mean element content ± standard deviations of at least five EDX spectral measurements.

as compared to the lignin extracted from WT and *lsi1* plants, indicating some variations in the self-assembly of the mutated polymer. The Lig-LowSi formed a more open network, as compared to Lig-HighSi. All lignin samples had residual Si, as detected by energy dispersive X-ray spectroscopy (EDX) elemental analysis. However, the average Si content was higher in Lig-HighSi than in Lig-LowSi (tables in Fig. 4). Interestingly, the fraction of oxygen was higher, and carbon was lower, in Lig-HighSi as compared to Lig-LowSi, suggesting that the functional groups were more oxidized in Lig-HighSi than in Lig-LowSi.

Pyrolysis of the extracted lignin occurred over a wide temperature range, from about 200 °C to 800 °C, with fast weight loss rate in parallel to the polysaccharide decomposition (stage (ii), 170–480 °C) (Fig. 2c, d and Table 1). Stage (ii) thermal decomposition of the isolated lignin, was divided into two maxima, at 254–269 °C and 338–350 °C. The first decomposition peak was associated with cleavage of aryl-alkyl ether (β-O-4) linkages to produce phenols and aromatic hydrocarbons.[40,41] This peak was bigger and shifted to higher temperatures in Lig-LowSi as compared to Lig-HighSi. Possibly, Lig-LowSi contained a higher fraction of ether bonds that broke to produce a higher concentration of volatile molecules, as compared to Lig-HighSi. The second peak was attributed to lignin side chain decomposition such as carboxylic acid and carbonyl group cleavage and oxidation, and dehydroxylation and hydroxyl cracking in lignin hydrogen bond networks.[40,41] This peak varied in lignin extracted from the different genotypes, possibly indicating variation in the distribution of side chain functional group content.

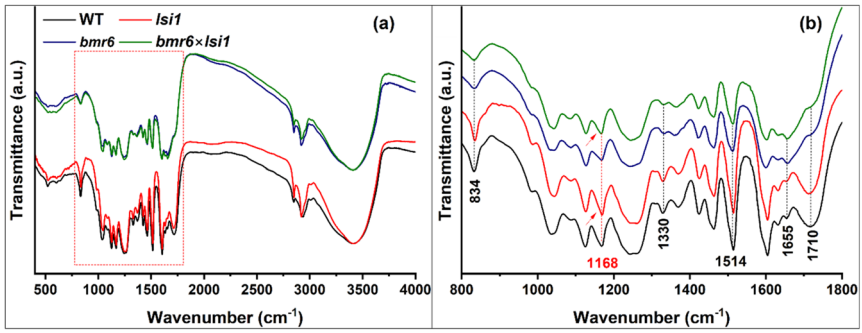

Fig. 5 FTIR transmission spectra of isolated lignin. Lignin extracted from wild type (WT, black), *lsi1* mutant (*lsi1*, red), *bmr6* mutant (*bmr6*, blue), and a double mutant in *lsi1* and *bmr6* (*lsi*×*bmr6*, green) sorghum genotypes, showing characteristic functional groups between 400 and 4000 cm^{-1} (a), and zoomed-in between 800 and 1800 cm^{-1} (b), as marked by a rectangle in panel (a). Structural differences in lignin, as a result of the *bmr6* mutation, are indicated by black vertical dotted lines. Conjugated carbonyl groups associated with silica–lignin interactions as a result of the *lsi1* mutation are indicated by the red vertical dotted line. Arrows indicate an increase in the absorption of these carbonyls in lignins of low-silicon as compared to native-silicon genotypes. See Table 2 for band assignments.

Fourier transform infrared (FTIR) spectroscopy of the isolated lignins indicated structural differences between the samples. The C=O stretch of conjugated aldehyde carbonyls at 1655 cm^{-1} was more abundant in mutated lignin extracted from *bmr6* and *bmr6*×*lsi1*, while non conjugated carbonyls of ketone and esters at 1710 cm^{-1} were abundant in lignin extracted from WT and *lsi1*. The intensities of absorptions assigned to S units at 834 cm^{-1} (C–H deformation) and 1330 cm^{-1} (C–O stretch) relative to the aromatic skeletal vibration at 1514 cm^{-1} were lower in mutated lignin (*bmr6* and *bmr6*×*lsi1*) compared to WT and *lsi1* lignin (Fig. 5 and Table 2). These results indicate that *bmr6* sorghum mutants have reduced S : G ratio, consistent with GC-MS results (Fig. 3) and the literature showing significantly reduced S-units and production of more aldehyde groups during biosynthesis in *bmr6* sorghum mutants.[31,48]

Plant silicon intake also affected the lignin FTIR signature. The strong absorption band at 3100–3600 cm^{-1}, attributed to the stretching vibrations of OH groups, was broader for Lig-HighSi as compared to Lig-LowSi (Fig. 5a). This could be attributed to a high concentration of hydroxyl moieties in Lig-HighSi on the expense of β-O-4 linkages, in agreement with the TGA and GC-MS results (Fig. 2 and 3). In accordance, the peak at 1168 cm^{-1} was bigger in Lig-LowSi compared to the corresponding Lig-HighSi (red arrows in Fig. 5b). This peak could be assigned to conjugated carbonyl moieties (C=O located at α position) and commonly observed in H–G–S type lignin.[45,49]

XPS of C 1s showed the presence of four species of carbon atoms with distinct binding energies (Fig. 6a). The C_1 peak at 285 eV corresponds to non-oxidized carbon (C–H, C–C, C=C); the C_2 peak at 286.5 eV corresponds to carbon bound to one oxygen through a single bond (C–OH, C–O–C); the C_3 peak at 288.2 eV corresponds to carbon bound to oxygen with two bonds (C=O), attributed to

Table 2 Assignment of infrared absorption bands of lignins, Si–O–C and Si–O–Si bonding vibration modes

Observed bands (cm^{-1})	Assignment	Source
3390–3435	O–H stretching	42 and 43
3005	C–H stretch of OCH_3	42 and 43
2935	Symmetric C–H stretch of OCH_3 and antisymmetric stretch of CH_2OH	42 and 43
2848	Symmetric C–H stretch of OCH_3	42 and 43
1710	C=O stretch of non-conjugated carbonyls	42 and 43
1654	C=O stretch of conjugated carbonyls	42 and 43
1630	O–H bending	42 and 43
1605	Aromatic ring stretch	42 and 43
1514	Aromatic ring stretch	42 and 43
1463	C–H bending of OCH_3 and CH_2	42 and 43
1423	Aromatic ring stretching with in plane C–H deformation	42 and 43
1369	Aliphatic C–H stretch in CH_3; not in OCH_3; phenolic OH	42 and 43
1330	C–O stretch of S ring; ring stretch of asymmetric-tetrasubstituted rings	42 and 43
1275	C–O stretch of G ring; C=O stretch	42 and 43
1265	C–O stretch of G ring; C=O stretch	42 and 43
1240	Si–phenoxy	44
1217	C–C, C–O, C=O stretch; G condensed > G etherified	42, 43 and 45
1204	C–C stretch	42, 43 and 45
1168	C=O stretch in ester group of HGS lignin	42, 43 and 45
1158	Si–O–C asymmetric stretching or C–O–Si cage link structure	44 and 46
1125	Aromatic C–H deformation of G units	42 and 43
1116	Si–O–C asymmetric stretching or C–O–Si open link structure	46
1085	C–O deformation in secondary alcohols and aliphatic ethers	42 and 43
1063	Si–O–C asymmetric stretching or C–O–Si ring link structure	44 and 46
1050	Si–O–Si asymmetric stretching of open chain siloxanes	44 and 46
1034	C–O deformation primary alcohols; C–O stretch of methoxy groups	42 and 43
1015	Si–O–Si asymmetric stretching of cyclic siloxanes	46
986	HC=CH out-of-plane deformation	42 and 43
975	Si–phenoxy	44
832	C–H bending of S units	42 and 43
523	Aromatic ring C–H deformation	42 and 43
469	Si–O–Si bending vibrations	47

carbonyls; and the C_4 peak at 289.2 eV corresponds to carbon with three bonds to oxygen (O–C=O), attributed to ester and carboxylic acid groups.[50,51]

The atomic ratio of carbon to oxygen (O/C) quantified by XPS was higher in Lig-HighSi than in Lig-LowSi (Table 3), in agreement with SEM-EDX results (Fig. 4). This may indicate a higher content of phenolic hydroxyls (C–OH) at the expense of β-O-4 ether bonds (C–O–C) in Lig-HighSi relative to Lig-LowSi, in accordance with the FTIR indication of increased hydroxyls in Lig-HighSi relative to Lig-LowSi (Fig. 5a). The lower fraction of C_3 in Lig-HighSi indicates that it may contain less carbonyls (C=O) than Lig-LowSi (Fig. 6a and Table 3). Interestingly, we noted

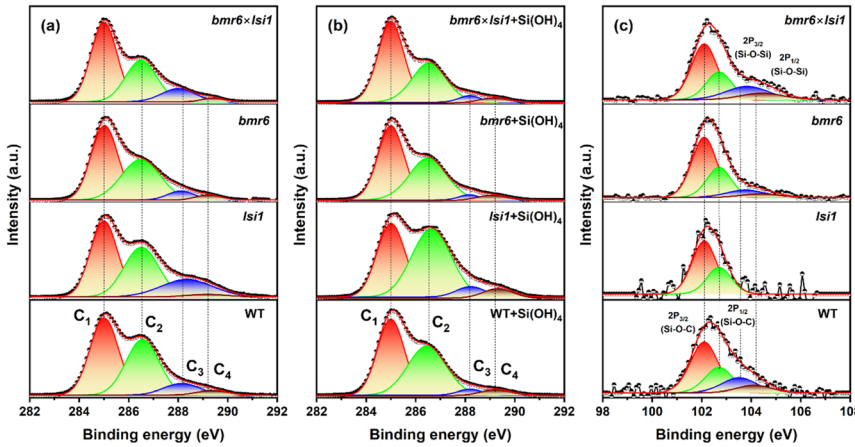

Fig. 6 High resolution XPS C 1s and Si 2p spectra of the four sorghum genotype lignins and lignin–silicic acid (lignin+Si) precipitates: (a) C 1s spectra of lignin extracted from WT, *lsi1*, *bmr6* and *bmr6*×*lsi1* sorghum genotypes. C_1 (C–C, CH, red), C_2, (C–OH, green) C_3 (O–C–O, C=O, blue), and C_4 (O–C=O, brown) peaks are deconvolved. (b) C 1s spectra of lignin+Si from WT, *lsi1*, *bmr6* and *bmr6*×*lsi1* sorghum genotypes precipitated with 2.5 mM silicic acid solution. Reduction in C_3 peaks (blue) with addition of silicic acid indicate reduction in C=O groups that possibly reacted to give Si–O–C. (c) Si 2p spectra of lignin extracted from WT, *lsi1*, *bmr6* and *bmr6*×*lsi1* sorghum genotypes. Lignin+Si samples showed similar Si 2p spectra with higher signal-to-noise ratio (Fig. S2†). Curves with filled area are deconvoluted peaks, the black-symbol curves represent the measured intensity, and the red curves represent the cumulative fit.

that the liquor extracted from BM-HighSi was less acidic than the liquor extracted from BM-LowSi (see Materials and methods, Section 2.4). This supports our analysis that Lig-HighSi contains a high fraction of phenolic hydroxyl groups (pK_a ~10) and low fraction of carbonyl groups (pK_a ~4.4).[52]

3.3 Identification of Si–O–C bonds and lignin potential to polymerize silicic acid

To study the chemistry between lignin and silica and to highlight possible Si–O–C bond formation, we reacted lignins with silicic acid solution (2.5, 5 mM) in

Table 3 XPS oxygen to carbon atomic concentration ratio (O/C) and percentage of assigned carbon species

	Percentage of carbon species (%)									
	O/C		C_1 (C–C, C–H, C=C)		C_2 (C–O)		C_3 (C=O, O–C–O)		C_4 (O–C=O)	
Samples	0 mM Si	2.5 mM Si	0 mM Si	2.5 mM Si	0 mM Si	2.5 mM Si	0 mM Si	2.5 mM Si	0 mM Si	2.5 mM Si
WT	0.29	0.3	48	48	40	45	9	4	3	4
lsi1	0.24	0.3	42	41	37	49	19	7	2	4
bmr6	0.26	0.3	51	52	40	42	6	3	3	3
bmr6×*lsi1*	0.22	0.3	53	56	33	37	12	4	2	3

phosphate buffer, herein lignin+Si. The solubility concentration of silicic acid in water is 1.7 mM,[53] above which, polymerisation to oligomeric silicic acid occurs. Therefore, we expected only minute amounts of silica polymerization. The C 1s XPS spectra of lignin+Si precipitates shows the reduction of C_3 (C=O, carbonyls) and the increase in C_2 (C–O, hydroxyls and ethers), compared to lignins that precipitated without silicic acid (Fig. 6a, b and Table 3). This suggests that the surface carbonyl moieties on the lignin reacted with silicic acid to give Si–O–C bonds. High resolution Si 2p spectra of lignin+Si were similar to lignin samples before silicic acid addition, however, with increased signal-to-noise ratio (Fig. 6c and S2†). Si–O–C bonds were detected in all samples, including lignin and lignin+Si, by the two major peaks at 102.1 eV (Si $2p_{3/2}$) and 102.7 eV (Si $2p_{1/2}$) (Fig. 6c), consistent with Si–O–C linkage.[54] In addition, two minor signals at 103.5 eV (Si $2p_{3/2}$) and 104.1 eV (Si $2p_{1/2}$) indicated Si–O–Si and Si–OH of silica (SiO_2).[55] Our results suggest that with the addition of silicic acid, surface Si–O–C and Si–O–Si bonds increased by a similar factor, while Si–O–C occupied most of the C=O positions in Lig-LowSi, reducing surface carbonyls significantly.

FTIR spectra of lignin+Si in comparison to the corresponding lignin exhibited an interesting variation in the band at 469 cm^{-1}, assigned to Si–O–Si bending modes. Under reaction with a marginally saturated silicic acid solution of 2.5 mM, lignin+Si spectra of only Lig-HighSi and not Lig-LowSi showed this peak. When silicic acid concentration was 5 mM it appeared in all lignin+Si samples, but its intensity was significantly higher in Lig-HighSi as compared to Lig-LowSi (Fig. 7). Further, pyrolysis residue during TGA of lignin+Si precipitates was found to be significantly higher in Lig-HighSi compared to Lig-LowSi (Fig. S3†). Our results indicated that Lig-HighSi has higher catalytic activity in polymerizing silicic acid. This could possibly occur through Si–phenoxyl bonds as Lig-HighSi contains higher free phenolics at the expense of β-O-4 linkages (Fig. 2 and 3) compared to Lig-LowSi.[17]

Supporting this, lignin extracted using the alkali pretreatment procedure in glass beakers showed a strong 469 cm^{-1} band only when extracted from BM-HighSi and not from BM-LowSi (ESI SI2 and Fig. S4†). This suggests that the Lig-HighSi could nucleate SiO_2 from silicic acid released from the glass beaker under alkaline pH, through binding silicic acid to the abundant phenolic hydroxyls and the formation of Si–phenoxyl bonds.

With the addition of silicic acid, we detected an increase in a shoulder at 975 cm^{-1} and a band at 1240 cm^{-1}, exclusively assigned to Si–O–phenoxyl[44] (Fig. 7 and Table 2). Further minor variations in the spectra could be attributed to Si–O–Si asymmetric stretching in cyclic siloxanes at 1015 cm^{-1}, open chain siloxanes at 1050 cm^{-1}, Si–O–C asymmetric stretching in the ring-link at 1063 cm^{-1}, open-link Si–O–C at 1116 cm^{-1}, and cage-link Si–O–C asymmetric stretching modes at 1158 cm^{-1}.[44,46]

In order to highlight these variations, we deconvoluted spectra of lignin and lignin+Si reacted with 2.5 mM silicic acid (Fig. 8). The area of the lignin bands at 1030 cm^{-1} assigned to C–O deformation of primary alcohols and methoxy groups, and at 1168 cm^{-1} assigned to conjugated C=O stretching, decreased with the addition of silicic acid, suggesting these bonds react with silicic acid. Fitted peaks assigned to Si–O–C bonds at 975, 1240, 1116 and 1158 cm^{-1}, and Si–O–Si bonds at 1050 cm^{-1} were observed in the spectra of all samples, and their relative integrated absorption area increased in lignin+Si precipitates. Two very small peaks, attributed

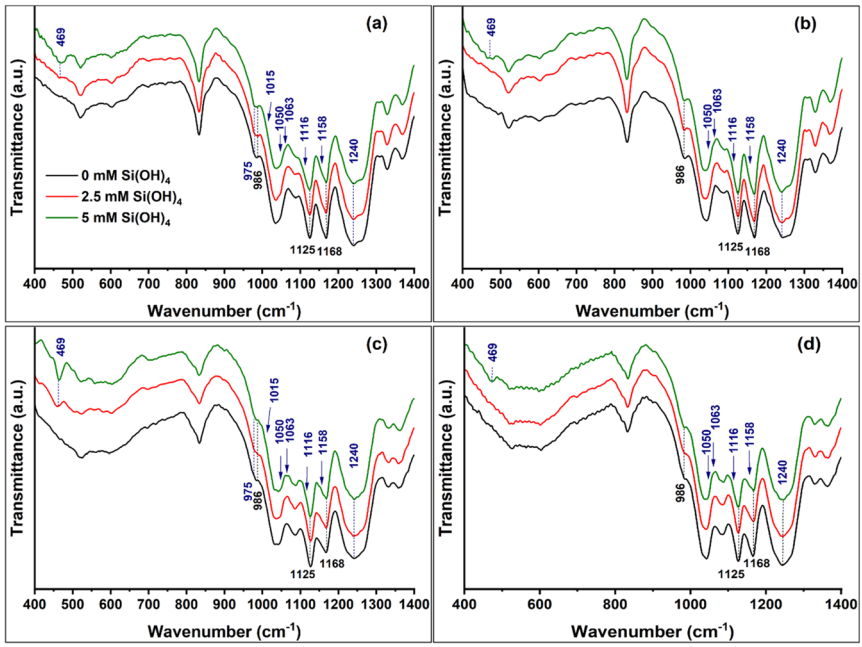

Fig. 7 FTIR transmission spectra of lignin and lignin+Si precipitants. Lignins extracted from biomass of (a) WT, (b) *lsi1*, (c) *bmr6* and (d) *bmr6*×*lsi1* plants (black lines) were reacted with silicic acid at 2.5 mM (red) and 5 mM (green) to form lignin+Si precipitates. Peaks and shoulder peaks of Si–O–Si and Si–O–C vibration modes are marked in blue text. Lignin major functional groups, marked in black text, overlapped with silica related peaks. Traces of Si–O–Si absorption band (469 cm^{-1}) appear when lignin reacted with 2.5 mM silicic acid only in WT and *bmr6*. This band is also stronger in lignins extracted from the biomass of WT and *bmr6* as compared to *lsi1* and *bmr6*×*lsi1* at 5 mM silicic acid.

to Si–O–Si asymmetric cyclic siloxane stretching (1015 cm^{-1}), and Si–O–C ring-link modes (1063 cm^{-1}) could be fitted only in the spectra of lignin+Si precipitates.

Based on the fit, we calculated the difference between the intensities of selected bands in lignin+Si and lignin samples (Fig. 9). As expected from our previous analysis (Fig. 7), with silicic acid addition, the increment in the integrated absorption area of the bands at 975 and 1240 cm^{-1} assigned to Si–O–phenoxyl bonding, was higher in Lig-HighSi compared to Lig-LowSi (Fig. 9a). Furthermore, the relative increase in the integrated absorption area of Si–O–Si asymmetric stretching in cyclic siloxanes (at 1016 cm^{-1}) and open chain siloxanes (at 1050 cm^{-1}) was greater in Lig-HighSi compared to Lig-LowSi (Fig. 9b).

Peaks related to the open-link Si–O–C bonds at 1116 cm^{-1} and cage-link Si–O–C bonds at 1158 cm^{-1} increased with the addition of silicic acid more in Lig-LowSi compared to Lig-HighSi (Fig. 9c). In parallel, a similar decrement was observed in the relative absorption of conjugated C=O stretching at 1168 cm^{-1}, and less so in C–O deformations at 1030 cm^{-1} (Fig. 9d). Taking into account the XPS results (Fig. 6a and b), the higher formation rate of Si–O–C with Lig-LowSi could be due to the availability of surface carbonyl groups to readily react with silicic acid and form Si–O–C bonds.

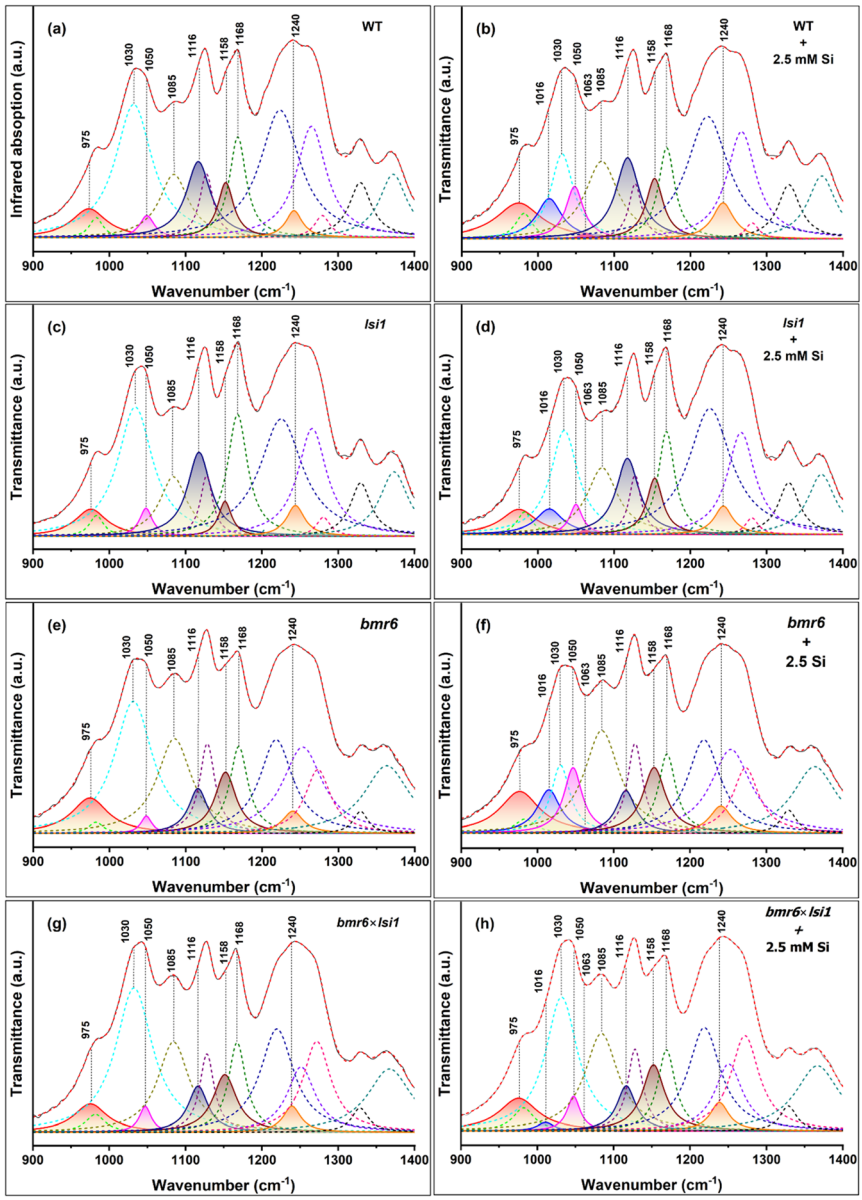

Fig. 8 Deconvolution of FTIR spectra of extracted lignin and lignin+Si reacted with 2.5 mM silicic acid. Si–O–C and Si–O–Si bonding modes are highlighted in the wavenumber range 950 to 1250 cm^{-1}. Spectra of lignin extracted from biomass of (a) WT, (c) *lsi1*, (e) *bmr6*, and (g) *bmr6*×*lsi1* plants were compared to lignin+Si precipitates of (b) WT, (d) *lsi1*, (f) *bmr6*, and (h) *bmr6*×*lsi1* plants. The black line represents infrared absorption, and red dashed line represents the cumulative peak fit of lignin (coloured-dashed lines) and Si–O (full lines with filled area).

3.4 Silica nanoparticle distribution in lignin of high-silicon genotypes

Tomography using scanning electron transmission microscopy (STEM) was performed in order to examine the distribution of silica within the agglomeration of

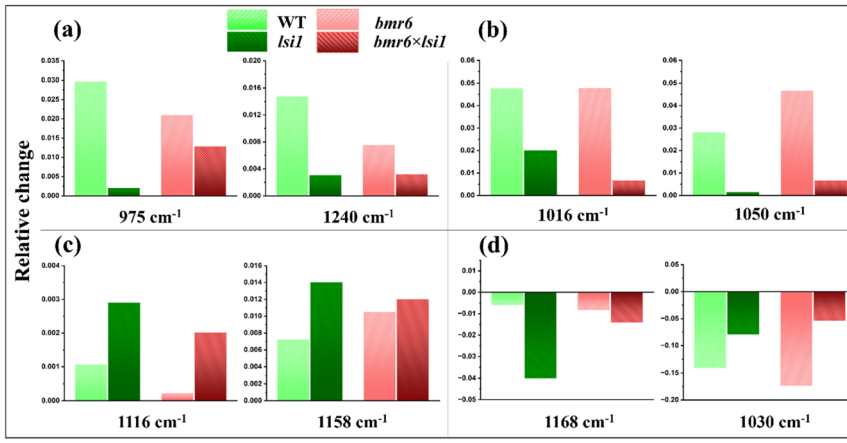

Fig. 9 Relative changes in the integrated absorption of lignin functional groups and Si–O–Si and Si–O–C modes in lignins from the different sorghum genotypes as a result of reaction with silicic acid. (a) Changes in bands at 975 and 1240 cm^{-1} assigned to the Si–O–C bonding modes in which Si is bonded to the phenoxyl group. (b) Changes in bands at 1016 cm^{-1}, assigned to Si–O–Si cyclic siloxanes, and at 1050 cm^{-1}, assigned Si–O–Si open chain siloxanes. (c) Changes in bands at 1116 and 1158 cm^{-1} assigned to open-link and cage-link Si–O–C bonds respectively. (d) Bands at 1168 cm^{-1}, assigned to conjugated C═O, and at 1030 cm^{-1}, assigned to C–O deformation in primary alcohols and methoxy groups, reduced with addition of silicic acid.

lignin particles. Specimens were prepared using lignin extracted from *bmr6* and *bmr6×lsi1* plants, both exposed to silicic acid solution of 2.5 mM concentration. Fig. 10 shows 60 nm thick virtual sections from the top, middle, and bottom of the specimens in a semi-transparent volume display mode (in addition, depth sectioning movies are provided in the ESI: video clips S1 and S2†). The two specimens appear as similar agglomerates of near-spherical particles some tens of nm in diameter forming a film of overall thickness 300–350 nm. Particles are clearly visible at the top and bottom of the clusters. They appear to have fused together near the central plane, but this may reflect a loss of resolution for boundaries and small channels within the bulk of the material. Notably, small dense particles of about 6–10 nm diameter appear near the mid-section of the *bmr6* specimen, but are absent in the *bmr6×lsi1*. Given the evidence from SEM-EDS, indicating a Si : C ratio of 3%, the small particles would not appear to account for all the silicon. Other silicon fractions could be bound as single or oligomeric silicic acid units dispersed within the lignin matrix. In order to investigate this, the same grids used for tomography were examined by the more sensitive STEM-EDS. A significant concentration of Si was found in the *bmr6* specimen, distributed throughout the lignin. Si was detected in the *bmr6×lsi1* specimen only at a level very close to background. These results establish strong evidence that lignin of the high silicon genotype, which has fewer β-O-4 linkages and free phenolics, effectively catalyse silicic acid to incorporate silica within the lignin matrix.

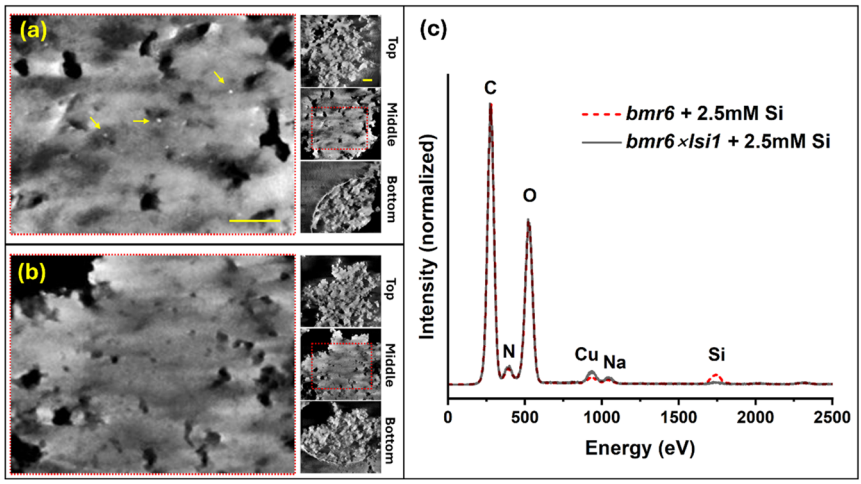

Fig. 10 Electron tomography of agglomerates of lignin extracted from *bmr6* and *bmr6*×*lsi1* plants, exposed to silicic acid at a concentration of 2.5 mM. (a) Thick virtual section reconstructed from the mid-plane of the *bmr6* specimen; note the dense nanoparticles indicated by yellow arrows, which we identify as silica deposits due to the strong electron scattering. Insets to the right show the top, middle, and bottom sections to indicate the texture of small, clustered particles of lignin at the top and bottom. The bright circular arc in the bottom section is the edge of a hole (2 μm diameter) in the specimen support film. (b) Virtual sections of the *bmr6*×*lsi1* specimen, organized as above. Bright nanoparticles were not observed. Scale bar in panel (a) is 200 nm, common to (a) and (b). Scale bar in the top inset is 200 nm, common to all insets. (c) EDX spectra recorded from the same grids, showing higher concentration of Si in the lignin extracted from the *bmr6* plant than the *bmr6*×*lsi1* plant.

4. Conclusions

The presented results indicate that Si–O–C bonds form primarily on lignin phenolic hydroxyls and conjugated carbonyl moieties either in the plant or during extraction. Lignin extracted from the biomass of plants with native-silicon intake showed a higher catalytic activity, polymerizing SiO_2 with higher content of Si–phenoxyl bonds, as compared to SiO_2 forming on lignin in low-silicon mutants. In synthetic lignin, the presence of phenoxy radicals and/or quinone methides of short lignin fragments have high affinity towards silica, and form cyclic siloxanes with Si–phenoxyl bonds instead of an extended Si–O–Si network.[17] The low content of β-O-4 ether linkages between monolignol units and high content of Si–O–Si formation with Lig-HighSi suggest that free phenolics (O-4) catalyse silicic acid condensation. In the *bmr6* genotype we measured higher SiO_2 content as compared to the WT genotype (Table 1 and Fig. 7), in agreement with our published data.[16] This could be explained by the increase in aliphatic carbonyl moieties forming under *bmr6* mutation, which enhance the catalytic activity of lignin in silicic acid condensation.

Interestingly, lignin and silica are not colocalized in the plant. Most lignin is polymerized in the vascular bundles, in xylem tracheary elements and fibre cells. In contrast, most silica is deposited at the epidermis, in silica cells and hairs and forming a double layer with the cuticle. Nonetheless, our work indicates

significant variations in the lignin structure as a result of silicic acid intake. The presented data indicate that silicic acid, when present in the apoplast, affects the radical dehydrogenation and polymerization of monolignols by capping the O-4 phenoxyl position. These positions are available in the polymerized lignin for H-bonding to other polymers and molecules and for binding cations. Such variations may explain some of the beneficial effects of silica in plants exposed to heavy metals.[56]

The presence of silicic acid during *in vivo* lignin polymerization apparently leads to the aryl-silyl ether (Si–O-4) bonds between silicic acid and monolignol phenoxyl radicals/quinone methides. This may lead to abundant phenoxyl Si–O–C bonds that effectively catalyse the polymerization of silicic acid into SiO_2 nanoparticles. In contrast, Lig-LowSi may be produced with abundant aryl-alkyl ether (β-O-4) bonds between monomers that would increase the cell wall density and the extension of conjugated carbonyls. This could explain the appearance of dense lignified cell walls with red-shifted autofluorescence in roots grown under low silicon conditions.[37] The common paradigm asserts that silica reduces biomass digestibility in parallel to lignin.[57,58] This work highlights a more complex relationship between the two materials as silica actually changes lignin, and *vice versa*. Extending this research will show whether the modified lignin has implications on the biological function of the tissue and valorisation of biomass.

Data availability

The STEM and STEM-EDX data that support the findings of this study are available under at **https://doi.org/10.5281/zenodo.14686717**.

Conflicts of interest

There are no conflicts to declare.

Acknowledgements

We thank Nerya Zexer for producing double mutant plants by crossing *bmr6* and *lsi1* sorghum plants, Shula Blum for isolating the homozygote *bmr6*×*lsi1* plants, and Lothar Houben for assistance with STEM-EDS. S. P. is thankful for a scholarship from Lady Davis and Golda Meir. This work was funded in part by the Israel Science Foundation grant 958/21. Contribution of ME was supported by the European Union (ERC, CryoSTEM, 101055413; Views and opinions expressed are however those of the authors only and do not necessarily reflect those of the European Union or the European Research Council. Neither the European Union nor the granting authority can be held responsible for them). ME is incumbent of the Sam and Ayala Zacks Professorial Chair in Chemistry.

References

1 L. A. Estroff, Introduction: Biomineralization, *Chem. Rev.*, 2008, **108**, 4329–4331.
2 R. Wood, Exploring the drivers of early biomineralization, *Emerging Top. Life Sci.*, 2018, **2**, 201–212.

3 P. U. P. A. Gilbert, K. D. Bergmann, N. Boekelheide, S. Tambutté, T. Mass, F. Marin, J. F. Adkins, J. Erez, B. Gilbert, V. Knutson, M. Cantine, J. Ortega Hernández and A. H. Knoll, Biomineralization: Integrating mechanism and evolutionary history, *Sci. Adv.*, 2022, **8**, 1–16.
4 N. Mitani-Ueno, N. Yamaji, S. Huang, Y. Yoshioka, T. Miyaji and J. F. Ma, *Nat. Commun.*, 2023, **14**, 6522.
5 J. D. Gargulak, S. E. Lebo and T. J. McNally, *Kirk-Othmer Encyclopedia of Chemical Technology*, Wiley, 2015, pp. 1–26.
6 S. Kumar, M. Soukup and R. Elbaum, *Front. Plant Sci.*, 2017, **8**, 438.
7 N. Zexer, S. Kumar and R. Elbaum, *Ann. Bot.*, 2023, **131**, 897–908.
8 Z. Lukačová, R. Švubová, J. Kohanová and A. Lux, *Plant Growth Regul.*, 2013, **70**, 89–103.
9 A. T. Fleck, T. Nye, C. Repenning, F. Stahl, M. Zahn and M. K. Schenk, *J. Exp. Bot.*, 2011, **62**, 2001–2011.
10 R. R. Rivai, K. Yamazaki, M. Kobayashi, Y. Tobimatsu, T. Tokunaga, T. Fujiwara and T. Umezawa, *Plant Cell Physiol.*, 2024, **65**, 1983–1992.
11 K. Radotić, D. Djikanović, A. Kalauzi, G. Tanasijević, V. Maksimović and J. Dragišić Maksimović, *Int. J. Biol. Macromol.*, 2022, **198**, 168–174.
12 J. Fang, H. Wang, Y. Chen and F. Zhang, *Prog. Nat. Sci.*, 2003, **13**, 501–504.
13 J. yu Fang and X. long Ma, *J. Zhejiang Univ., Sci., B*, 2006, **7**, 267–271.
14 M. Soukup, V. M. Rodriguez Zancajo, J. Kneipp and R. Elbaum, *J. Exp. Bot.*, 2020, **71**, 6807–6817.
15 C. Zhang, L. Wang, W. Zhang and F. Zhang, *Plant Soil*, 2013, **372**, 137–149.
16 N. Zexer and R. Elbaum, *J. Exp. Bot.*, 2022, **73**, 1450–1463.
17 S. Palakurthy, L. Houben, M. Elbaum and R. Elbaum, *Biomacromolecules*, 2024, **25**, 3409–3419.
18 D. Delmer, R. A. Dixon, K. Keegstra and D. Mohnen, *Plant Cell*, 2024, **36**, 1257–1311.
19 J. H. Coomey, R. Sibout and S. P. Hazen, *New Phytol.*, 2020, **227**, 1649–1667.
20 L. Salmén, *Cellulose*, 2022, **29**, 1349–1355.
21 J. Gierer, *Wood Sci. Technol.*, 1985, **19**, 289–312.
22 J. Snelders, E. Dornez, B. Benjelloun-Mlayah, W. J. J. Huijgen, P. J. de Wild, R. J. A. Gosselink, J. Gerritsma and C. M. Courtin, *Bioresour. Technol.*, 2014, **156**, 275–282.
23 H. Labauze, N. Cachet and B. Benjelloun-Mlayah, *Ind. Crops Prod.*, 2022, **187**, 115328.
24 F. Abdelkafi, H. Ammar, B. Rousseau, M. Tessier, R. El Gharbi and A. Fradet, *Biomacromolecules*, 2011, **12**, 3895–3902.
25 Q. Zheng, L. Chai, B. Du, W. Li, L. H. Fu and X. Chen, *Polymers*, 2023, **15**, 1867.
26 I. Tari, G. Laskay, Z. Takács and P. Poór, *J. Agron. Crop Sci.*, 2013, **199**, 264–274.
27 W. L. Rooney, J. Blumenthal, B. Bean and J. E. Mullet, *Biofuels, Bioprod. Biorefin.*, 2007, **1**, 147–157.
28 S. Głazowska, L. Baldwin, J. Mravec, C. Bukh, T. H. Hansen, M. M. Jensen, J. U. Fangel, W. G. T. Willats, M. Glasius, C. Felby and J. K. Schjoerring, *Biotechnol. Biofuels*, 2018, **11**(171), 1–18.
29 A. G. Sangster and D. W. Parry, *Ann. Bot.*, 1976, **40**, 361–371.
30 O. Markovich, S. Kumar, D. Cohen, S. Addadi, E. Fridman and R. Elbaum, *Silicon*, 2019, **11**, 2385–2391.

31 E. D. Scully, T. Gries, D. L. Funnell-Harris, Z. Xin, F. A. Kovacs, W. Vermerris and S. E. Sattler, *J. Integr. Plant Biol.*, 2016, **58**, 136–149.
32 Z. Peleg, Y. Saranga, T. Fahima, A. Aharoni and R. Elbaum, *Physiol. Plant.*, 2010, **140**, 10–20.
33 A. E. Harman-Ware, C. Foster, R. M. Happs, C. Doeppke, K. Meunier, J. Gehan, F. Yue, F. Lu and M. F. Davis, *Biotechnol. J.*, 2016, **11**, 1268–1273.
34 S. Seifer, L. Houben and M. Elbaum, *Microsc. Microanal.*, 2021, **27**, 1476–1487.
35 D. N. Mastronarde and S. R. Held, *J. Struct. Biol.*, 2017, **197**, 102–113.
36 T. Emiola-Sadiq, L. Zhang and A. K. Dalai, *ACS Omega*, 2021, **6**, 22233–22247.
37 N. Zexer and R. Elbaum, *J. Exp. Bot.*, 2020, **71**, 6818–6829.
38 J. Ralph and J. H. Grabber, *Holzforschung*, 1996, **50**, 425–428.
39 C. Lapierre, B. Pollet, B. Monties and C. Rolando, *Holzforschung*, 1991, **45**, 61–68.
40 T. Faravelli, A. Frassoldati, G. Migliavacca and E. Ranzi, *Biomass Bioenergy*, 2010, **34**, 290–301.
41 X. Lu and X. Gu, *Biotechnol. Biofuels*, 2022, **15**, 106.
42 R. J. Sammons, D. P. Harper, N. Labbé, J. J. Bozell, T. Elder and T. G. Rials, *BioResources*, 2013, **8**, 2752–2767.
43 P. Bock, P. Nousiainen, T. Elder, M. Blaukopf, H. Amer, R. Zirbs, A. Potthast and N. Gierlinger, *J. Raman Spectrosc.*, 2020, **51**, 422–431.
44 L. J. Bellamy, *The Infra-red Spectra of Complex Molecules*, Chapman and Hall, London, 1975, pp. 374–384.
45 T. You and F. Xu, *Applications of Molecular Spectroscopy to Current Research in the Chemical and Biological Sciences*, InTech, 2016, pp. 235–260, DOI: **10.5772/64581**.
46 G. L. L. Barry Arkles, *Silicon Compounds – Silanes and Silicones*, Gelest, Morrisville, USA, 3rd edn, 2013.
47 R. Al-Oweini and H. El-Rassy, *J. Mol. Struct.*, 2009, **919**, 140–145.
48 S. E. Sattler, D. L. Funnell-Harris and J. F. Pedersen, *J. Agric. Food Chem.*, 2010, **58**, 3611–3616.
49 H. L. Hergert and E. F. Kurth, *J. Org. Chem.*, 1953, **18**, 521–529.
50 J. Wang, K. Yao, A. L. Korich, S. Li, S. Ma, H. J. Ploehn, P. M. Iovine, C. Wang, F. Chu and C. Tang, *J. Polym. Sci., Part A: Polym. Chem.*, 2011, **49**, 3728–3738.
51 C. M. Popescu, C. M. Tibirna and C. Vasile, *Appl. Surf. Sci.*, 2009, **256**, 1355–1360.
52 M. Ragnar, C. T. Lindgren and N. O. Nilvebrant, *J. Wood Chem. Technol.*, 2000, **20**, 277–305.
53 R. K. Iler, *The Chemistry of Silica : Solubility, Polymerization, Colloid and Surface Properties, and Biochemistry*, Wiley, New York, 7th edn, 1979.
54 A. Avila, I. Montero, L. Galán, J. M. Ripalda and R. Levy, *J. Appl. Phys.*, 2001, **89**, 212–216.
55 G. Dakroub, T. Duguet, J. Esvan, C. Lacaze-Dufaure, S. Roualdes and V. Rouessac, *Surf. Interfaces*, 2021, **25**, 101256.
56 B. Bokor, C. S. Santos, D. Kostoláni, J. Machado, M. N. da Silva, S. M. P. Carvalho, M. Vaculík and M. W. Vasconcelos, *J. Hazard. Mater.*, 2021, **416**, 126193.
57 P. J. Van Soest and L. H. P. Jones, *J. Dairy Sci.*, 1968, **51**, 1644–1648.
58 M. P. Silva, C. Whitehead, R. L. Ordonio, T. C. Fernando, M. P. B. Castillo, J. L. Ordonio, T. Larson, D. J. Upton, S. E. Hartley and L. D. Gomez, *Biomass Bioenergy*, 2024, **182**, 107099.